Russ. J. Numer. Anal. Math. Modelling, Vol. 24, No. 6, pp. 543–563 (2009)
DOI 10.1515/ RJNAMM.2009.034

Uzawa method on semi-staggered grids for unsteady Bingham media flows

L. V. MURAVLEVA* and E. A. MURAVLEVA†

Abstract — A finite difference scheme on semi-staggered grids is used for numerical simulation of unsteady flows of an incompressible viscoplastic Bingham medium. The Duvaut–Lions variational inequality is considered as a mathematical model. The convergence of the Uzawa method is proved. The efficiency of the method is demonstrated on a model problem with a known exact solution (plane Poiseuille flow) and on the unsteady driven cavity problem.

1. Statement of the problem

There exists a number of materials behaving as a viscoplastic medium (Bingham medium), namely, i.e., the medium behaves as a rigid body below some limit stress value and above this level it behaves as an incompressible viscous fluid. A variational statement for the flows of viscoplastic media was first proposed by Il'yushin [11]. In [16] the existence and uniqueness theorems were proved for the problem of the flow in a pipe and a qualitative study of flow specifics was performed. Monograph [8] contains strict mathematical analysis of variational inequalities corresponding to this model.

Let Ω be a bounded domain in $R^d, d = 2, 3$, and Γ be a locally Lipschitz boundary of the domain Ω. A flow of an incompressible viscoplastic medium during the time interval $(0, T)$ is described by the following system of equations and constitutive relations:

$$\rho\left[\frac{\partial \mathbf{v}}{\partial t} + (\mathbf{v}\cdot\nabla)\mathbf{v}\right] = \nabla\cdot\boldsymbol{\sigma} + \mathbf{f}, \quad \nabla\cdot\mathbf{v} = 0 \quad \text{in } \Omega\times(0,T) \tag{1.1}$$

$$\boldsymbol{\sigma} = -p\mathbf{I} + \boldsymbol{\tau}, \quad \boldsymbol{\tau} = \begin{cases} 2\mu\mathbf{D}(\mathbf{v}) + \sigma_s\dfrac{\mathbf{D}(\mathbf{v})}{|\mathbf{D}(\mathbf{v})|}, & |\mathbf{D}(\mathbf{v})| \neq 0 \\ |\boldsymbol{\tau}| \leqslant \sigma_s, & |\mathbf{D}(\mathbf{v})| = 0 \end{cases} \tag{1.2}$$

$$\mathbf{v}(0) = \mathbf{v}_0 \quad \text{in } \Omega, \quad \nabla\cdot\mathbf{v}_0 = 0, \quad \mathbf{v} = \mathbf{0} \quad \text{on } \Gamma\times(0,T). \tag{1.3}$$

*Moscow State University, Faculty of Mechanics and Mathematics, Moscow 119991, Russia
†Institute of Numerical Mathematics, Russian Academy of Sciences, Moscow 119333, Russia
The work was partially supported by the Russian Foundation for Basic Research (08–01–00353, 09–01–00565).

Equations (1.1)–(1.3) use the standard notations: ρ, μ, σ_s are positive constants, namely the density, the viscosity coefficient, and the yield stress of the Bingham medium, respectively (sometimes we use τ_s as shear yield stress, $\sigma_s = \tau_s\sqrt{2}$); $\mathbf{v}$ is the unknown velocity field, $\mathbf{f}$ is the given field of external forces; $\boldsymbol{\sigma}$ is the stress tensor, $\boldsymbol{\tau}$ is the deviator of the stress tensor, and p is the pressure, $\mathbf{D}(\mathbf{v}) = [\nabla\mathbf{v} + (\nabla\mathbf{v})^T]/2$ is the strain rate tensor with the norm $|\mathbf{D}(\mathbf{v})| = \left(\sum_{i=1}^d \sum_{j=1}^d D_{ij}(\mathbf{v}) D_{ij}(\mathbf{v})\right)^{1/2}$.

System (1.1)–(1.3) holds in the domain of motion (i.e., $|\mathbf{D}(\mathbf{v})| > 0$) and, generally speaking, has no meaning in the rigid zone $\Omega_0 = \left\{\{\mathbf{x}, t\} \in \Omega \times (0,T) \,|\, |\mathbf{D}(\mathbf{v})(\mathbf{x},t)| = 0\right\}$. The typical peculiarity in problems of viscoplastic media flows is the necessity to construct solutions in domains with unknown boundaries. This causes significant difficulties in construction of efficient methods for their study. The main difficulty in numerical simulation of the flow of a viscoplastic medium is related to nondifferentiability of constitutive relations. One of the most successful techniques to overcome the mentioned difficulties is using the theory of variational inequalities [8, 10, 12]. The finite element method is traditionally employed as the discretization technique [7] in numerical simulation of Bingham media. In this paper we apply the finite-difference scheme from [19–23] for determination of an approximate solution. We consider the numerical solution of the unsteady driven cavity problem for a Bingham medium as a model example. The obtained results are compared to those known from the literature.

2. Variational inequality

Duvaut and Lions [8] proposed the problem on the solvability of following variational inequality (2.1) (with conditions (2.2),(2.3)) as a strict formulation of problem (1.1)–(1.3) of a viscoplastic flow: determine $\mathbf{v}(t) \in (H_0^1(\Omega))^d$ so that for each $t \in (0,T)$ the following inequality holds:

$$\begin{aligned} &\rho \int_\Omega \frac{\partial \mathbf{v}}{\partial t} \cdot (\mathbf{u} - \mathbf{v}(t))\mathrm{d}\mathbf{x} + \rho \int_\Omega (\mathbf{v}(t)\cdot\nabla)\mathbf{v}(t) \cdot (\mathbf{u} - \mathbf{v}(t))\mathrm{d}\mathbf{x} \\ &\quad + 2\mu \int_\Omega \mathbf{D}(\mathbf{v}(t)) : \mathbf{D}(\mathbf{u} - \mathbf{v}(t))\mathrm{d}\mathbf{x} + \sigma_s \int_\Omega (|\mathbf{D}(\mathbf{u})| - |\mathbf{D}(\mathbf{v}(t))|)\mathrm{d}\mathbf{x} \\ &\geqslant \int_\Omega \mathbf{f}(t) \cdot (\mathbf{u} - \mathbf{v}(t))\mathrm{d}\mathbf{x} \quad \forall \mathbf{u} \in \mathbf{U} \end{aligned} \tag{2.1}$$

$$\nabla \cdot \mathbf{v}(t) = 0 \quad \text{in } \Omega, \quad \mathbf{v}(0) = \mathbf{v}_0 \quad \text{in } \Omega, \quad \mathbf{v}(t) = 0 \quad \text{on } \Gamma \tag{2.2}$$

$$\mathbf{U} = \{\mathbf{u} \in (H^1(\Omega))^d \,|\, \nabla \cdot \mathbf{u} = 0\} \tag{2.3}$$

where $\mathbf{A} : \mathbf{B} = \sum_{i=1}^d \sum_{j=1}^d a_{ij} b_{ij}$ for all tensors $\mathbf{A} = (a_{ij})$ and $\mathbf{B} = (b_{ij})$ of the second order. Inequality (2.1) 'automatically' includes the problem on a 'free boundary'. In our case it is the surface separating the domain in which the flow is described by equation (1.1) from the domain where the medium moves as a rigid body. The following theorem on multipliers was also proved in [8].

Theorem 2.1 [8]. *Let* $\mathbf{v}$ *be a solution to problem* (2.1)–(2.3)*. Then there exists a tensor-valued function* $\boldsymbol{\lambda} = \{\lambda_{ij}\}_{1\leqslant i,j\leqslant d}$ *such that*

$$\boldsymbol{\lambda} \in (L^\infty(\Omega))^{d\times d}, \quad \boldsymbol{\lambda} = \boldsymbol{\lambda}^T, \quad |\boldsymbol{\lambda}| \leqslant 1$$
$$\boldsymbol{\lambda} : \mathbf{D}(\mathbf{v}) = |\mathbf{D}(\mathbf{v})|, \ \ a.e.\ in\ \ \Omega\times(0,T) \tag{2.4}$$
$$\rho\left[\frac{\partial \mathbf{v}}{\partial t} + (\mathbf{v}\cdot\nabla)\mathbf{v}\right] - \mu\triangle\mathbf{v} - \sigma_s\nabla\cdot\boldsymbol{\lambda} + \nabla p = \mathbf{f} \ \ in\ \ \Omega\times(0,T) \tag{2.5}$$
$$\nabla\cdot\mathbf{v} = 0\ in\ \Omega\times(0,T), \quad \mathbf{v}(0) = \mathbf{v}_0\ \ in\ \ \Omega, \quad \mathbf{v} = 0 \ \ on\ \ \Gamma\times(0,T). \tag{2.6}$$

If, on the contrary, the triple $\{\mathbf{v}, p, \boldsymbol{\lambda}\}$ *satisfies relations* (2.4)–(2.6)*, then* $\mathbf{v}$ *is the solution to problem* (2.1)–(2.3)*.*

3. Discretization of problem (2.1)–(2.3) in time

Suppose the flow is slow, i.e., we can neglect the convective term (the Stokes approximation). Following [7], we use the well-known backward Euler scheme for time discretization of problem (2.1)–(2.3). Let $\triangle t > 0$ be a constant time step. Assume

$$\mathbf{v}^0 = \mathbf{v}_0$$

then for $k \geqslant 1$ we compute $\mathbf{v}^k$ from $\mathbf{v}^{k-1}$ as the solution to the following inequality (here and further $\mathbf{f}^k = \mathbf{f}(k\triangle t)$)

$$\frac{\rho}{\triangle t}\int_\Omega (\mathbf{v}^k - \mathbf{v}^{k-1})\cdot(\mathbf{u}-\mathbf{v}^k)\mathrm{d}\mathbf{x} + 2\mu\int_\Omega \mathbf{D}(\mathbf{v}^k) : \mathbf{D}(\mathbf{u}-\mathbf{v}^k)\mathrm{d}\mathbf{x}$$
$$+ \sigma_s\int_\Omega (|\mathbf{D}(\mathbf{u})| - |\mathbf{D}(\mathbf{v}^k)|)\mathrm{d}\mathbf{x} \geqslant \int_\Omega \mathbf{f}^k\cdot(\mathbf{u}-\mathbf{v}^k)\mathrm{d}\mathbf{x} \quad \forall\mathbf{u}\in\mathbf{U}.$$

We introduce $\alpha = \rho/\triangle t, \mathbf{f} = \mathbf{f}^k + \alpha\mathbf{v}^{k-1}$, in what follows we omit the subscript k. Then in the new notations we have

$$\alpha\int_\Omega \mathbf{v}\cdot(\mathbf{u}-\mathbf{v})\mathrm{d}\mathbf{x} + 2\mu\int_\Omega \mathbf{D}(\mathbf{v}) : \mathbf{D}(\mathbf{u}-\mathbf{v})\mathrm{d}\mathbf{x} + \sigma_s\int_\Omega (|\mathbf{D}(\mathbf{u})| - |\mathbf{D}(\mathbf{v})|)\mathrm{d}\mathbf{x}$$
$$\geqslant \int_\Omega \mathbf{f}\cdot(\mathbf{u}-\mathbf{v})\mathrm{d}\mathbf{x} \quad \forall\mathbf{u}\in\mathbf{U}. \tag{3.1}$$

4. Uzawa's algorithm

Numerical methods for solving variational inequality (3.1) are based on the following approach. Introduce the functional

$$J(\mathbf{u}) = \frac{\alpha}{2}\int_\Omega |\mathbf{u}|^2\mathrm{d}\mathbf{x} + \mu\int_\Omega |\mathbf{D}(\mathbf{u})|^2\mathrm{d}\mathbf{x} + \sigma_s\int_\Omega |\mathbf{D}(\mathbf{u})|\mathrm{d}\mathbf{x} - \int_\Omega \mathbf{f}\cdot\mathbf{u}\,\mathrm{d}\mathbf{x}. \tag{4.1}$$

The functional $J(\mathbf{u})$ is strictly convex, but is not differentiable because of the term $\sigma_s \int_\Omega |\mathbf{D}(\mathbf{u})| \mathrm{d}\mathbf{x}$. The solution $\mathbf{v}$ of problem (3.1) is the minimiser of the functional J on $\mathbf{U}$ [10]:

$$\mathbf{v} = \arg\min_{\mathbf{u}\in\mathbf{U}} J(\mathbf{u}). \tag{4.2}$$

Taking into account inequality (2.4), for the integral of the contraction $\boldsymbol{\lambda} : \mathbf{D}(\mathbf{u})$,

$$\int_\Omega \boldsymbol{\lambda} : \mathbf{D}(\mathbf{u}) \mathrm{d}\mathbf{x} \leqslant \int_\Omega |\boldsymbol{\lambda}||\mathbf{D}(\mathbf{u})| \mathrm{d}\mathbf{x} \leqslant \int_\Omega |\mathbf{D}(\mathbf{u})| \mathrm{d}\mathbf{x} \quad \forall \mathbf{u} \in (H_0^1(\Omega))^d$$
$$\int_\Omega \boldsymbol{\lambda} : \mathbf{D}(\mathbf{v}) \mathrm{d}\mathbf{x} = \int_\Omega |\mathbf{D}(\mathbf{v})| \mathrm{d}\mathbf{x}$$

we get the following relation:

$$\int_\Omega |\mathbf{D}(\mathbf{v})| \mathrm{d}\mathbf{x} = \sup_{\boldsymbol{\lambda}\in\boldsymbol{\Lambda}} \int_\Omega \boldsymbol{\lambda} : \mathbf{D}(\mathbf{v}) \mathrm{d}\mathbf{x} \tag{4.3}$$

where $\boldsymbol{\Lambda} = \{\boldsymbol{\lambda} | \boldsymbol{\lambda} \in (L^\infty(\Omega))^{d\times d},\ \boldsymbol{\lambda} = \boldsymbol{\lambda}^T,\ |\boldsymbol{\lambda}| \leqslant 1 \text{ a.e. on } \Omega\}$. Further, substituting expression (4.3) into the functional, we have

$$\inf_{\mathbf{u}\in\mathbf{U}} \left(\frac{\alpha}{2} \int_\Omega |\mathbf{u}|^2 \mathrm{d}\mathbf{x} + \mu \int_\Omega |\mathbf{D}(\mathbf{u})|^2 \mathrm{d}\mathbf{x} + \sigma_s \sup_{\boldsymbol{\lambda}\in\boldsymbol{\Lambda}} \int_\Omega \boldsymbol{\lambda} : \mathbf{D}(\mathbf{u}) \mathrm{d}\mathbf{x} - \int_\Omega \mathbf{f}\cdot\mathbf{u}\, \mathrm{d}\mathbf{x} \right)$$

or

$$\inf_{\mathbf{u}\in\mathbf{U}} \sup_{\boldsymbol{\lambda}\in\boldsymbol{\Lambda}} \left(\frac{\alpha}{2} \int_\Omega |\mathbf{u}|^2 \mathrm{d}\mathbf{x} + \mu \int_\Omega |\mathbf{D}(\mathbf{u})|^2 \mathrm{d}\mathbf{x} + \sigma_s \int_\Omega \boldsymbol{\lambda} : \mathbf{D}(\mathbf{u}) \mathrm{d}\mathbf{x} - \int_\Omega \mathbf{f}\cdot\mathbf{u}\, \mathrm{d}\mathbf{x} \right).$$

Introduce the Lagrange functional $\mathscr{L} : (H^1(\Omega))^d \times (L^2(\Omega))^{d\times d} \to \mathbb{R}$ corresponding to (4.1) as

$$\mathscr{L}(\mathbf{u};\boldsymbol{\eta}) = \frac{\alpha}{2} \int_\Omega |\mathbf{u}|^2 \mathrm{d}\mathbf{x} + \mu \int_\Omega |\mathbf{D}(\mathbf{u})|^2 \mathrm{d}\mathbf{x} + \sigma_s \int_\Omega \boldsymbol{\eta} : \mathbf{D}(\mathbf{u}) \mathrm{d}\mathbf{x} - \int_\Omega \mathbf{f}\cdot\mathbf{u}\, \mathrm{d}\mathbf{x}. \tag{4.4}$$

In accordance with the minimax theorem [9, 10], the pair $(\mathbf{v}, \boldsymbol{\lambda})$ is a saddle point of the Lagrange functional $\mathscr{L}(\mathbf{u};\boldsymbol{\eta})$ on $\mathbf{U}\times\boldsymbol{\Lambda}$:

$$(\mathbf{v}, \boldsymbol{\lambda}) \in U_B \times \boldsymbol{\Lambda}, \quad \mathscr{L}(\mathbf{v};\boldsymbol{\eta}) \leqslant \mathscr{L}(\mathbf{v};\boldsymbol{\lambda}) \leqslant \mathscr{L}(\mathbf{u};\boldsymbol{\lambda}) \quad \forall (\mathbf{u}, \boldsymbol{\eta}) \in \mathbf{U}\times\boldsymbol{\Lambda} \tag{4.5}$$

and the first component of the pair $\mathbf{v}$ is uniquely determined and it is the solution to optimization problem (4.2). The first inequality of (4.5) is equivalent [9, 26] to the equation

$$\boldsymbol{\lambda}(t) = P_{\boldsymbol{\Lambda}}(\boldsymbol{\lambda}(t) + r\sigma_s \mathbf{D}(\mathbf{v}(t))) \quad \forall r > 0, \text{ a.e. on } \Omega\times(0,T) \tag{4.6}$$

where $P_{\mathbf{\Lambda}} : (L^\infty(\Omega))^{d\times d} \to \mathbf{\Lambda}$ is the operator of orthogonal projection defined by the following expression:

$$P_{\mathbf{\Lambda}}(\mathbf{q})(x) = \begin{cases} \mathbf{q}(x), & |\mathbf{q}(x)| \leqslant 1 \\ \mathbf{q}(x)/|\mathbf{q}(x)|, & |\mathbf{q}(x)| > 1 \end{cases}, \text{ a.e. on } \Omega \quad \forall \mathbf{q} \in (L^\infty(\Omega))^{d\times d}. \tag{4.7}$$

This remark plays an important role in computations. Due to Theorem 2.1, the pair $(\mathbf{v}, \boldsymbol{\lambda})$ satisfies the following relations:

$$\alpha\mathbf{v} - 2\mu\nabla\cdot\mathbf{D}(\mathbf{v}) - \sigma_s\nabla\cdot\boldsymbol{\lambda} + \nabla p = \mathbf{f}, \quad \nabla\cdot\mathbf{v} = 0 \ \text{ in } \Omega, \quad \mathbf{v} = \mathbf{0} \ \text{ on } \Gamma \tag{4.8}$$

$$\boldsymbol{\lambda} = P_{\mathbf{\Lambda}}(\boldsymbol{\lambda} + r\sigma_s\mathbf{D}(\mathbf{v})). \tag{4.9}$$

Based on (4.8)–(4.9), we construct the following algorithm, which is the Uzawa algorithm applied to the saddle-point problem with $\mathscr{L}(\mathbf{u};\boldsymbol{\eta})$:

$$\boldsymbol{\lambda}^0 \in \mathbf{\Lambda} \text{ is given (arbitrarily)} \tag{4.10}$$

for $n \geqslant 0$, assuming that $\boldsymbol{\lambda}^n (\in \mathbf{\Lambda})$ is known, we compute $\mathbf{v}^n$ as an element of $\mathbf{U}$ that is the saddle point of the Lagrangian $\mathscr{L}(\mathbf{u};\boldsymbol{\eta})$, i.e., as the solution to the problem

$$\alpha\mathbf{v}^n - 2\mu\nabla\cdot\mathbf{D}(\mathbf{v}^n) - \sigma_s\nabla\cdot\boldsymbol{\lambda}^n + \nabla p^n = \mathbf{f}, \quad \nabla\cdot\mathbf{v} = 0 \ \text{ in } \Omega, \quad \mathbf{v} = \mathbf{0} \ \text{ on } \Gamma \tag{4.11}$$

after that, the new approximation $\boldsymbol{\lambda}^{n+1}$ is determined as

$$\boldsymbol{\lambda}^{n+1} = P_{\mathbf{\Lambda}}(\boldsymbol{\lambda}^n + r\sigma_s\mathbf{D}(\mathbf{v}^n)). \tag{4.12}$$

The following remark presents several useful formulae we need further in the proof of the theorem.

Remark 4.1. Considering the velocity gradient $\nabla\mathbf{v}$ as a second-order tensor, represent it in the form of a sum of the symmetric strain rate tensor $\mathbf{D}(\mathbf{v})$ and the antisymmetric rotation velocity tensor $\mathbf{w}(\mathbf{v}) = \frac{1}{2}\left[\nabla\mathbf{v} - (\nabla\mathbf{v})^T\right]$ with the components $(w_{ij} = \frac{1}{2}(\nabla_i v_j - \nabla_j v_i))$. Then, taking into account that the contraction of the symmetric and antisymmetric tensors is equal to zero, we get the following relations:

$$\mathbf{D}(\mathbf{v}) : \mathbf{w}(\mathbf{v}) = 0, \quad \boldsymbol{\lambda} : \mathbf{w}(\mathbf{v}) = 0 \quad (\boldsymbol{\lambda} = \boldsymbol{\lambda}^T).$$

In addition, for $\mathbf{D}(\mathbf{v}) : \nabla\mathbf{v}$ and $\boldsymbol{\lambda} : \nabla\mathbf{v}$ we have

$$\begin{aligned} \mathbf{D}(\mathbf{v}) : \nabla\mathbf{v} &= \sum_{i,j=1}^{d} D_{ij}(\mathbf{v})\nabla_i v_j = \sum_{i,j=1}^{d} D_{ij}(\mathbf{v})(D_{ij}(\mathbf{v}) + w_{ij}(\mathbf{v})) \\ &= \sum_{i,j=1}^{d} D_{ij}(\mathbf{v})D_{ij}(\mathbf{v}) = |\mathbf{D}(\mathbf{v})|^2 \\ \boldsymbol{\lambda} : \nabla\mathbf{v} &= \sum_{i,j=1}^{d} \lambda_{ij}(D_{ij}(\mathbf{v}) + w_{ij}(\mathbf{v})) = \sum_{i,j=1}^{d} \lambda_{ij}D_{ij}(\mathbf{v}) = \boldsymbol{\lambda} : \mathbf{D}(\mathbf{v}). \end{aligned}$$

Prove the theorem of convergence of Uzawa's method for problem (2.1)–(2.3).

Theorem 4.1. *Suppose the condition*

$$0 < r < 4\mu/\sigma_s^2 \tag{4.13}$$

holds. Then for the sequence $\{\mathbf{v}^n\}_{n\geqslant 0}$ *generated by algorithm* (4.10)–(4.12) *we have*

$$\lim_{n\to+\infty} \mathbf{v}^n = \mathbf{v} \quad in \ (H_0^1(\Omega))^d$$

where $\mathbf{v}$ *is the solution to* (4.8)–(4.9).

Proof. Let $\{\mathbf{v},\boldsymbol{\lambda}\}$ be the solution to (4.8)–(4.9). Assuming $\overline{\mathbf{v}}^n = \mathbf{v}^n - \mathbf{v}, \overline{p}^n = p^n - p$ and $\overline{\boldsymbol{\lambda}}^n = \boldsymbol{\lambda}^n - \boldsymbol{\lambda}$ and taking into account that the projection operator $P_{\boldsymbol{\Lambda}}$ satisfies the relation $\|P_{\boldsymbol{\Lambda}}x - P_{\boldsymbol{\Lambda}}y\| \leqslant \|x-y\|$, as a result of subtraction of (4.8)–(4.9) from (4.11)–(4.12), we get that for all $n \geqslant 0$ we have

$$\alpha\overline{\mathbf{v}}^n - 2\mu\nabla\cdot\mathbf{D}(\overline{\mathbf{v}}^n) - \sigma_s\nabla\cdot\overline{\boldsymbol{\lambda}}^n + \nabla\overline{p}^n = 0, \ \nabla\cdot\overline{\mathbf{v}}^n = 0 \text{ in } \Omega, \ \overline{\mathbf{v}}^n = 0 \text{ on } \Gamma \tag{4.14}$$

$$\|\overline{\boldsymbol{\lambda}}^{n+1}\|_{(L^2(\Omega))^{d\times d}} \leqslant \|\overline{\boldsymbol{\lambda}}^n + r\sigma_s\mathbf{D}(\overline{\mathbf{v}}^n)\|_{(L^2(\Omega))^{d\times d}}. \tag{4.15}$$

Inequality (4.15) implies

$$\|\overline{\boldsymbol{\lambda}}^{n+1}\|^2_{(L^2(\Omega))^{d\times d}} \leqslant \|\overline{\boldsymbol{\lambda}}^n\|^2_{(L^2(\Omega))^{d\times d}} + 2r\sigma_s(\overline{\boldsymbol{\lambda}}^n, \mathbf{D}(\overline{\mathbf{v}}^n)) + r^2\sigma_s^2\|\mathbf{D}(\overline{\mathbf{v}}^n)\|^2_{(L^2(\Omega))^{d\times d}}$$

which gives

$$\|\overline{\boldsymbol{\lambda}}^n\|^2_{(L^2(\Omega))^{d\times d}} - \|\overline{\boldsymbol{\lambda}}^{n+1}\|^2_{(L^2(\Omega))^{d\times d}} \geqslant -r^2\sigma_s^2\|\mathbf{D}(\overline{\mathbf{v}}^n)\|^2_{(L^2(\Omega))^{d\times d}} - 2r\sigma_s(\overline{\boldsymbol{\lambda}}^n, \mathbf{D}(\overline{\mathbf{v}}^n)). \tag{4.16}$$

Multiply (4.14) by $\overline{\mathbf{v}}^n$:

$$(\alpha\overline{\mathbf{v}}^n, \overline{\mathbf{v}}^n) - 2\mu(\nabla\cdot\mathbf{D}(\overline{\mathbf{v}}^n), \overline{\mathbf{v}}^n) - \sigma_s(\nabla\cdot\overline{\boldsymbol{\lambda}}^n, \overline{\mathbf{v}}^n) + (\nabla\overline{p}^n, \overline{\mathbf{v}}^n) = 0$$

integrate by parts, and take into account Remark 4.1:

$$\alpha\|\overline{\mathbf{v}}^n\|^2_{(L^2(\Omega))^2} + 2\mu(\mathbf{D}(\overline{\mathbf{v}}^n), \mathbf{D}(\overline{\mathbf{v}}^n)) + \sigma_s(\overline{\boldsymbol{\lambda}}^n, \mathbf{D}(\overline{\mathbf{v}}^n)) = 0$$

because of

$$(\nabla\cdot\mathbf{D}(\overline{\mathbf{v}}^n), \overline{\mathbf{v}}^n) = -(\mathbf{D}(\overline{\mathbf{v}}^n), \nabla\overline{\mathbf{v}}^n) = -(\mathbf{D}(\overline{\mathbf{v}}^n), \mathbf{D}(\overline{\mathbf{v}}^n)) = -\|\mathbf{D}(\overline{\mathbf{v}}^n)\|^2_{(L^2(\Omega))^{d\times d}}$$

$$(\nabla\cdot\overline{\boldsymbol{\lambda}}^n, \overline{\mathbf{v}}^n) = -(\overline{\boldsymbol{\lambda}}^n, \nabla\overline{\mathbf{v}}^n) = -(\overline{\boldsymbol{\lambda}}^n, \mathbf{D}(\overline{\mathbf{v}}^n)).$$

For all $\mathbf{v}$ such that $\mathbf{v} \in (H_0^1(\Omega))^d$, $\nabla\cdot\mathbf{v} = 0$ we have $2\|\mathbf{D}(\mathbf{v})\|^2_{(L^2(\Omega))^{d\times d}} = \|\nabla\mathbf{v}\|^2_{(L^2(\Omega))^{d\times d}}$ because of

$$2(\mathbf{D}(\mathbf{v}),\mathbf{D}(\mathbf{v})) = 2(\mathbf{D}(\mathbf{v}),\nabla\mathbf{v}) = 2\sum_{i,j=1}^{d}(D_{ij},\nabla_i v_j) = \sum_{i,j=1}^{d}(\nabla_i v_j + \nabla_j v_i,\nabla_i v_j)$$
$$= \sum_{i,j=1}^{d}(\nabla_i v_j,\nabla_i v_j) + \sum_{i,j=1}^{d}(\nabla_j v_i,\nabla_i v_j) = \|\nabla\mathbf{v}\|^2 - \sum_{i,j=1}^{d}(\nabla_i\nabla_j v_i, v_j)$$
$$= \|\nabla\mathbf{v}\|^2 - \sum_{j=1}^{d}\Big(\nabla_j\Big(\sum_{i=1}^{d}\nabla_i v_i\Big), v_j\Big) = \|\nabla\mathbf{v}\|^2_{(L^2(\Omega))^{d\times d}}.$$

Thus,

$$2r\alpha\|\overline{\mathbf{v}}^n\|^2_{(L^2(\Omega))^d} + 4r\mu\|\mathbf{D}(\overline{\mathbf{v}}^n)\|^2_{(L^2(\Omega))^{d\times d}} = -2r\sigma_s(\overline{\boldsymbol{\lambda}}^n,\mathbf{D}(\overline{\mathbf{v}}^n)). \tag{4.17}$$

Taking into account relations (4.16) and (4.17), we get

$$\|\overline{\boldsymbol{\lambda}}^n\|^2_{(L^2(\Omega))^{d\times d}} - \|\overline{\boldsymbol{\lambda}}^{n+1}\|^2_{(L^2(\Omega))^{d\times d}}$$
$$\geqslant -r^2\sigma_s^2\|\mathbf{D}(\overline{\mathbf{v}}^n)\|^2_{(L^2(\Omega))^{d\times d}} + 2r\alpha\|\overline{\mathbf{v}}^n\|^2_{(L^2(\Omega))^d} + 4r\mu\|\mathbf{D}(\overline{\mathbf{v}}^n)\|^2_{(L^2(\Omega))^{d\times d}}$$
$$= 2r(\|\mathbf{D}(\overline{\mathbf{v}}^n)\|^2_{(L^2(\Omega))^{d\times d}}(2\mu - r\sigma_s^2/2) + \alpha\|\overline{\mathbf{v}}^n\|^2_{(L^2(\Omega))^d})$$
$$= r(\|\nabla(\overline{\mathbf{v}}^n)\|^2_{(L^2(\Omega))^{d\times d}}(2\mu - r\sigma_s^2/2) + 2\alpha\|\overline{\mathbf{v}}^n\|^2_{(L^2(\Omega))^d})$$
$$= r\Big(\|\nabla(\overline{\mathbf{v}}^n)\|^2_{(L^2(\Omega))^{d\times d}}\mu\Big(2 - \frac{r\sigma_s^2}{2\mu}\Big) + \alpha\Big(2 - \frac{r\sigma_s^2}{2\mu} + \frac{r\sigma_s^2}{2\mu}\Big)\|\overline{\mathbf{v}}^n\|^2_{(L^2(\Omega))^d}\Big)$$
$$\geqslant r\Big(2 - \frac{r\sigma_s^2}{2\mu}\Big)(\mu\|\nabla(\overline{\mathbf{v}}^n)\|^2_{(L^2(\Omega))^{d\times d}} + \alpha\|\overline{\mathbf{v}}^n\|^2_{(L^2(\Omega))^d}). \tag{4.18}$$

Condition (4.13) implies $r(2 - r\sigma_s^2/2\mu) > 0$ (where, as we have seen, $\alpha = \rho/\Delta t$). Relations (4.18) imply that the sequence $\big(\|\overline{\boldsymbol{\lambda}}^n\|^2_{(L^2(\Omega))^{d\times d}}\big)_{n\geqslant 0}$ decreases and hence converges to some limit. The latter means

$$\lim_{n\to+\infty}\big(\|\overline{\boldsymbol{\lambda}}^n\|^2_{(L^2(\Omega))^{d\times d}} - \|\overline{\boldsymbol{\lambda}}^{n+1}\|^2_{(L^2(\Omega))^{d\times d}}\big) = 0. \tag{4.19}$$

Combining (4.18) and (4.19), we get $\lim_{n\to+\infty}\overline{\mathbf{v}}^n = 0$ in $(H^1(\Omega))^d$, namely, the convergence of $\{\mathbf{v}^n\}_{n\geqslant 0}$ to $\mathbf{v}$ in $(H_0^1(\Omega))^d$.

Remark 4.2. Estimate (4.13) determines the interval of admissible values of the parameter r providing the convergence of Uzawa's algorithm (projection method) to the solution. But in the proof of Theorem 4.1 we neglect the term $\alpha\|\overline{\mathbf{v}}^n\|^2_{(L^2(\Omega))^d}$ in formula (4.18). Estimate (4.13) allows us to choose a value of r both for steady and unsteady problems. For evolutional problems the range of admissible values of

the parameter r may be extended a little. According to the Poincaré inequality, the following relation holds:

$$\gamma_{\min}\|\mathbf{v}\|^2_{(L^2(\Omega))^d} \leqslant \|\nabla\mathbf{v}\|^2_{(L^2(\Omega))^{d\times d}}$$

where $\gamma_{\min}$ is the least eigenvalue of the Laplace operator with the homogeneous Dirichlet boundary conditions in the domain Ω. Replacing in (4.18) the value $\|\nabla(\overline{\mathbf{v}}^n)\|^2_{(L^2(\Omega))^{d\times d}}$ by a smaller expression containing only $\|\overline{\mathbf{v}}^n\|^2_{(L^2(\Omega))^{d\times d}}$, we get

$$\begin{aligned} &r(\|\nabla(\overline{\mathbf{v}}^n)\|^2_{(L^2(\Omega))^{d\times d}}(2\mu - r\sigma_s^2/2) + 2\alpha\|\overline{\mathbf{v}}^n\|^2_{(L^2(\Omega))^d}) \\ &\quad\geqslant r\big(\gamma_{\min}\|\overline{\mathbf{v}}^n\|^2_{(L^2(\Omega))^{d\times d}}(2\mu - r\sigma_s^2/2) + 2\alpha\|\overline{\mathbf{v}}^n\|^2_{(L^2(\Omega))^d}\big) \\ &\quad= r\|\overline{\mathbf{v}}^n\|^2_{(L^2(\Omega))^{d\times d}}\Big(2\mu - \frac{r\sigma_s^2}{2} + \frac{2\alpha}{\gamma_{\min}}\Big)\gamma_{\min}. \end{aligned}$$

Thus, the extended interval of admissible values for the parameter r has the form

$$0 < r < 4/\sigma_s^2(\mu + \alpha/\gamma_{\min}).$$

5. Finite-difference scheme

The Uzawa method described in Section 4 is applicable to the finite-difference approximation of variational inequality (3.1). Further we restrict ourselves to the case of a rectangular domain Ω. Since the Uzawa method is justified here in its functional form, its application to a finite-dimensional problem cannot be assumed completely justified. This gap will be filled in one of the forthcoming papers. As it was pointed out in Section 1, most papers concerning numerical simulation of a Bingham medium use the finite element method for discretization [14]. In [19–22] some difference schemes were proposed, and one of those schemes is used in this paper. Let $\Omega = (0,1)^2$ and assume $h_1 = N_1^{-1}$ and $h_2 = N_2^{-1}$ for given natural N_1, N_2. Define the following grid domains:

$$\bar{\Omega}_1 = \{x_{ij} = (ih_1, jh_2) \mid i = 0,\dots,N_1, j = 0,\dots,N_2\}$$

$$\Omega_2 = \{x_{ij} = ((i+1/2)h_1, (j+1/2)h_2) \mid i = 0,\dots,N_1-1, j = 0,\dots,N_2-1\}.$$

Define the spaces of the grid components of the velocity and pressure functions taking real values:

$$\begin{aligned} &\mathbf{V}_h^0 = \{\mathbf{v}_{i,j} = (u_{i,j}, v_{i,j}) = (u(x_{ij}), v(x_{ij})) \mid x_{ij} \in \bar{\Omega}_1,\ \mathbf{v}_{0,j} = \mathbf{v}_{i,N_2} = \mathbf{v}_{N_1,j} = \mathbf{v}_{i,0} = \mathbf{0}\} \\ &P_h = \{p_{ij} := p(x_{ij}) \mid x_{ij} \in \Omega_2,\ \sum_{i,j} p_{ij} = 0\}. \end{aligned}$$

By $\mathbf{V}_h$ we denote the spaces of the grid vector functions determined only at the internal points of Ω_1. All components of the strain rate tensor $(\mathbf{D}_h(\mathbf{v}_h) = \{\mathbf{D}_h(\mathbf{v}_h)\}_{i,j})$

and the stress tensor ($\boldsymbol{\lambda}_h = \{\boldsymbol{\lambda}_h\}_{i,j}$) are determined on the grid Ω_2. The corresponding space of real grid tensor functions is denoted by $\mathbf{Q}_h$:

$$\mathbf{Q}_h = \{\mathbf{q}_h \mid \mathbf{q}_h = \{q_h^{11}, q_h^{12}, q_h^{21}, q_h^{22}\};\ (\mathbf{q}_h)_{i,j} = \mathbf{q}_h(x_{ij}),\ x_{ij} \in \Omega_2\}.$$

For vector grid functions of the form $\mathbf{v}_h = (u, v)^T$ determined on $\bar{\Omega}_1$ we define the scalar product by the formula

$$(\mathbf{u}_h, \mathbf{v}_h)_h = \sum_{x_{ij} \in \bar{\Omega}_1} (u^1_{i,j} u^2_{i,j} + v^1_{i,j} v^2_{i,j}) h_1 h_2, \quad \mathbf{u}_h = (u^1, v^1)^T, \quad \mathbf{v}_h = (u^2, v^2)^T$$

for scalar functions determined on Ω_2 we use the formula

$$(p_h, q_h)_h = \sum_{x_{ij} \in \Omega_2} p_{i,j} q_{i,j} h_1 h_2$$

for tensor functions determined on Ω_2 we use the formula

$$(\mathbf{q}_h, \boldsymbol{\lambda}_h)_h = \sum_{x_{ij} \in \Omega_2} (q^{11}_{i,j} \lambda^{11}_{i,j} + q^{12}_{i,j} \lambda^{12}_{i,j} + q^{21}_{i,j} \lambda^{21}_{i,j} + q^{22}_{i,j} \lambda^{22}_{i,j}) h_1 h_2.$$

Further in the text we use norms for vector, scalar, and tensor grid functions. All those norms are calculated based on the introduced scalar products:

$$\|\mathbf{v}_h\|_h = (\mathbf{v}_h, \mathbf{v}_h)_h^{1/2}, \quad \|p_h\|_h = (p_h, p_h)_h^{1/2}, \quad \|\boldsymbol{\lambda}_h\|_h = (\boldsymbol{\lambda}_h, \boldsymbol{\lambda}_h)_h^{1/2}.$$

Define the discrete analogue of the differential divergence operator $\nabla_h \cdot : \mathbf{V}_h^0 \to P_h$:

$$(\nabla_h \cdot \mathbf{v}_h)_{i,j} = \frac{u_{i+1,j+1} - u_{i,j+1} + u_{i+1,j} - u_{i,j}}{2h_1} + \frac{v_{i+1,j+1} - v_{i+1,j} + v_{i,j+1} - v_{i,j}}{2h_2} \tag{5.1}$$

and the strain rate tensor $\mathbf{D}_h : \mathbf{V}_h^0 \to \mathbf{Q}_h$:

$$\begin{aligned}
(D_h^{11}(\mathbf{v}_h))_{i,j} &= \frac{u_{i+1,j+1} - u_{i,j+1} + u_{i+1,j} - u_{i,j}}{2h_1} \\
(D_h^{22}(\mathbf{v}_h))_{i,j} &= \frac{v_{i+1,j+1} - v_{i+1,j} + v_{i,j+1} - v_{i,j}}{2h_2} \\
(D_h^{12}(\mathbf{v}_h))_{i,j} &= (D_h^{21}(\mathbf{v}_h))_{i,j} = \frac{u_{i+1,j+1} - u_{i+1,j} + u_{i,j+1} - u_{i,j}}{4h_2} \\
&\quad + \frac{v_{i+1,j+1} - v_{i,j+1} + v_{i+1,j} - v_{i,j}}{4h_1}.
\end{aligned}$$

A direct check verifies that the difference scheme obtained here approximates the original problem with the order $\mathcal{O}(h^2)$ for smooth functions. Define a closed convex set $\boldsymbol{\Lambda}_h$ and spaces $\mathbf{Q}_h$ by

$$\boldsymbol{\Lambda}_h = \{\boldsymbol{\lambda}_h \mid \boldsymbol{\lambda}_h \in \mathbf{Q}_h,\ \boldsymbol{\lambda}_h = \boldsymbol{\lambda}_h^T, |\boldsymbol{\lambda}_h| \leqslant 1\}$$

$|\boldsymbol{\lambda}_h|_{i,j} = ((\lambda_h^{11})_{i,j}^2 + 2(\lambda_h^{12})_{i,j}^2 + (\lambda_h^{22})_{i,j}^2)^{1/2}$ is the norm of a tensor function at a point $x_{ij} \in \Omega_2$.

Consider the discrete analogue of the Lagrangian $\mathscr{L}(\mathbf{u};\boldsymbol{\eta})$ (4.4):

$$\mathscr{L}_h(\mathbf{v}_h, \boldsymbol{\lambda}_h) = h_1 h_2 \left[\frac{\alpha}{2} \sum_{M_{ij} \in \Omega_1} \left((u_h)^2 + (v_h)^2 \right) + \mu \sum_{M_{ij} \in \Omega_2} \left((D_h^{11})^2 + (D_h^{22})^2 + 2(D_h^{12})^2 \right) \right.$$
$$\left. + \sigma_s \sum_{M_{ij} \in \Omega_2} \left(D_h^{11}\lambda_h^{11} + D_h^{22}\lambda_h^{22} + 2D_h^{12}\lambda_h^{12} \right) - \sum_{M_{ij} \in \Omega_1} \left(f_h^1 u_h + f_h^2 v_h \right) \right].$$

In order to find the saddle point of the discrete Lagrangian $\mathscr{L}_h(\mathbf{v}_h, \boldsymbol{\lambda}_h)$, we apply the discrete version of algorithm (4.10)–(4.12) in the following form:

$$\boldsymbol{\lambda}_h^0 \in \boldsymbol{\Lambda}_h \text{ is given arbitrarily}$$

given $\boldsymbol{\lambda}_h^n (\in \boldsymbol{\Lambda}_h)$, $n \geqslant 0$, we compute $\mathbf{v}_h^n$, after that the new approximation $\boldsymbol{\lambda}_h^{n+1}$ is determined by the following steps.

Step 1. Solve

$$\begin{cases} \alpha \mathbf{v}_h^n - \mu \triangle_h \mathbf{v}^n + \nabla_h p_h^n = \sigma_s \nabla_h \cdot \boldsymbol{\lambda}_h^n + \mathbf{f}_h \\ \nabla_h \cdot \mathbf{v}_h^n = 0. \end{cases} \tag{5.2}$$

Step 2. Calculate

$$\boldsymbol{\lambda}_h^{n+1} = P_{\boldsymbol{\Lambda}_h}(\boldsymbol{\lambda}_h^n + r\sigma_s \mathbf{D}_h(\mathbf{v}_h^n)). \tag{5.3}$$

If $\|\boldsymbol{\lambda}_h^{n+1} - \boldsymbol{\lambda}_h^n\| > \varepsilon$, then repeat from Step 1.

For the discretizations $(\nabla_h \cdot \mathbf{v}_h)$ and $(\mathbf{D}_h(\mathbf{v}_h))$ introduced here and under the condition $\nabla_h \cdot \mathbf{v}_h = 0$, the following equality holds:

$$2(\mathbf{D}_h(\mathbf{v}_h), \mathbf{D}_h(\mathbf{v}_h)) = (\nabla_h \mathbf{v}_h, \nabla_h \mathbf{v}_h) = (-\triangle_h \mathbf{v}_h, \mathbf{v}_h). \tag{5.4}$$

In this case we obtain the following discrete analogues of the gradient operator $\nabla_h : P_h \to \mathbf{V}_h$:

$$(\nabla_h p_h)_{i,j} = \left(\frac{p_{i,j} - p_{i-1,j} + p_{i,j-1} - p_{i-1,j-1}}{2h_1}, \frac{p_{i,j} - p_{i,j-1} + p_{i-1,j} - p_{i-1,j-1}}{2h_2} \right) \tag{5.5}$$

and the Laplace operator $\Delta_h : \mathbf{V}_h^0 \to \mathbf{V}_h$:

$$(\Delta_h \mathbf{v}_h)_{i,j} = \frac{1}{4h_1^2}(\mathbf{v}_{i+1,j+1} - 2\mathbf{v}_{i,j+1} + \mathbf{v}_{i-1,j+1}$$
$$+ 2\mathbf{v}_{i+1,j} - 4\mathbf{v}_{i,j} + 2\mathbf{v}_{i-1,j} + \mathbf{v}_{i+1,j-1} - 2\mathbf{v}_{i,j-1} + \mathbf{v}_{i-1,j-1})$$
$$+ \frac{1}{4h_2^2}(\mathbf{v}_{i+1,j+1} + 2\mathbf{v}_{i,j+1} + \mathbf{v}_{i-1,j+1}$$
$$- 2\mathbf{v}_{i+1,j} - 4\mathbf{v}_{i,j} - 2\mathbf{v}_{i-1,j} + \mathbf{v}_{i+1,j-1} + 2\mathbf{v}_{i,j-1} + \mathbf{v}_{i-1,j-1}).$$

In the case $h_1 = h_2 = h$ for Δ_h we obtain the so-called 'shift' approximation:

$$(\Delta_h \mathbf{v}_h)_{i,j} = \frac{\mathbf{v}_{i-1,j-1} + \mathbf{v}_{i+1,j-1} + \mathbf{v}_{i+1,j+1} + \mathbf{v}_{i-1,j+1} - 4\mathbf{v}_{i,j}}{2h^2}. \tag{5.6}$$

The choice of the parameter r in algorithm (5.2), (5.3) is performed in formal accordance with Remark 4.2, i.e., we suppose $\|\nabla_h \mathbf{v}_h^n\|_h$ converges to $\|\nabla_h \mathbf{v}_h\|_h$ for all r from the interval

$$0 < r < \frac{4}{\sigma_s^2}\Big(\mu + \frac{\alpha}{\gamma_{\min}}\Big).$$

Before proceeding to numerical experiments, let us discuss the algorithm and the details of its implementation. The second step performs pointwise calculations and causes no difficulties. The first step consists in the solution of the generalized Stokes problem with a constant matrix of the system and a variable right-hand side. The first iterative methods for solution of the stationary Stokes problem in the 'pressure-velocity' variables were the Arrow–Hurwitz and Uzawa methods. In spite of the fact that more than fifty years have passed since the creation of these methods, they remain to be the basis for the development of new iterative methods [1, 5]. Consider the system of grid equations for the stationary Stokes problem

$$\begin{aligned} -\Delta_h \mathbf{v}_h + \nabla_h p_h &= \mathbf{F}_h \\ \nabla_h \cdot \mathbf{v}_h &= 0. \end{aligned}$$

If the system is not degenerate, then applying the Uzawa method, we first solve the equation for pressure $S_h p_h = \varphi$,

$$S_h p_h \equiv \nabla_h \cdot \Delta_h^{-1} \nabla_h p_h = \nabla_h \cdot \Delta_h^{-1} \mathbf{F}_h \equiv \varphi$$

and then calculate the velocity $\mathbf{v}_h$,

$$\mathbf{v}_h = (\Delta_h)^{-1}(\mathbf{F}_h - \nabla_h p_h).$$

In the case when S_h is degenerate, we require the fulfillment of the condition $\varphi \perp \ker \nabla_h$. Then the problem is solvable and the normal solution should be orthogonal to the kernel of the discrete gradient operator.

It is well known that for the Stokes problem the difference scheme with operators (5.1), (5.5), (5.6) constructed here leads to a degenerate matrix S_h. In order to ascertain that, note that even in the two-dimensional case the discrete gradient operator ∇_h (5.5) has (in contrast to the continuous case) a nontrivial kernel of the form

$$\mathrm{Ker}(\nabla_h) = \mathrm{span}(p^1, p^2), \quad p^1_{i,j} = (-1)^{i+j} - 1, \quad p^2_{i,j} = (-1)^{i+j+1} - 1 \tag{5.7}$$

in the space P_h. Therefore, the operator S_h has a nontrivial kernel on P_h. In this case one of the standard methods for solving system (5.2) is the solution of the equation $S_h p_h = \varphi$ in the subspace of the space P_h orthogonal to $\mathrm{Ker}(\nabla_h)$ (5.7). However, in

the three-dimensional case the dimension of the kernel increases with a decreasing h [18], and such approach becomes not very efficient. Several authors [25] used staggered grids for calculation of the flow of a viscous incompressible fluid and in this case a special additional term was included into the equation for the pressure. This term is in some sense equivalent to the addition of a biharmonic operator into the continuity equation.

In order to stabilize the scheme on semi-staggered grids, we apply the approach proposed recently in [3] for stabilization of LBB-unstable elements $Q_1 - Q_0$ possessing an explicit analogy with this difference scheme. This approach consists in supplementing the Lagrangian of the Stokes problem by the term $-\int_\Omega (p - \Pi p)^2 \, d\mathbf{x}$, where Π is some operator of local interpolation from P_h into the space of piecewise-bilinear continuous functions.

Define the operator $\Pi_h : P_h \to R_h$, where R_h is the space of grid functions determined on $\bar{\Omega}_1$. Let $x_{ij} \in \Omega_1$. Denote

$$\omega(x_{ij}) = \left\{ x_{kl} \in \Omega_2 \mid |x_{kl} - x_{ij}| = \frac{1}{2}(h_x^2 + h_y^2)^{1/2} \right\}$$

then

$$(\Pi_h p_h)_{ij} = |\omega(x_{ij})|^{-1} \sum_{x_{kl} \in \omega(x_{ij})} p_{kl}.$$

The operator Π_h may be considered as the grid 'interpolation' of the function given on the grid Ω_2 by a function determined on the grid Ω_1. Let Π_h^* be the operator conjugate to the Euclidean scalar product. Assume $G_h = (I_h - \Pi_h^* \Pi_h)$, $G_h : P_h \to P_h$. Taking into account the stabilizing term, the continuity equation $\nabla \cdot \mathbf{v} = 0$ is approximated on the grid Ω_2 in the following way: $\nabla_h \cdot \mathbf{v}_h + G_h p_h = 0$. If the grid is uniform, then $G_h = h^2 \Delta_h^p / 4$, where Δ_h^p is the approximation of the Laplace operator with the Neumann boundary conditions having a nine-point stencil (in the two-dimensional case):

$$\begin{pmatrix} \frac{1}{16} & \frac{1}{8} & \frac{1}{16} \\ \frac{1}{8} & -\frac{3}{4} & \frac{1}{8} \\ \frac{1}{16} & \frac{1}{8} & \frac{1}{16} \end{pmatrix}.$$

Thus, the stabilizing term has the second order in h on smooth solutions. The system of algebraic equations for the solution of Stokes problem (5.2) takes the following form for the constructed scheme:

$$\begin{pmatrix} A & B \\ B^T & -C \end{pmatrix} \begin{pmatrix} \mathbf{v} \\ p \end{pmatrix} = \begin{pmatrix} \mathbf{f} \\ \mathbf{g} \end{pmatrix}.$$

The matrix is sparse and has a block structure. The mathematical analysis of this scheme is the subject of a separate paper [23]. Note that the proposed stabilization is applicable to the three-dimensional case too.

6. Numerical experiments

The first step of algorithm (5.2) consists in the solution of the Stokes problem. Therefore, at first we present the results of numerical experiments for known analytic solutions in the square $(0,1)^2$. Taking into account that the kernel of the discrete gradient operator is nontrivial, we compare the two methods described above, namely, determination of the solution on the subspace orthogonal to the kernel and the use of the scheme with the stabilizing term.

6.1. Trigonometric polynomial (viscous fluid)

Let us consider the solution:

$$\begin{aligned} u &= \frac{1}{4\pi^2}(1-\cos 2\pi x)\sin 2\pi y \\ v &= \frac{1}{4\pi^2}\sin 2\pi x(1-\cos 2\pi y) \\ p &= \frac{1}{\pi}\sin 2\pi x \sin 2\pi y. \end{aligned} \tag{6.1}$$

The calculation results are presented in Tables 1 and 2. Table 1 corresponds to the orthogonalization method, Table 2 corresponds to the stabilized scheme. The tables present the values of the error norms for the velocity $\mathbf{e}_h = \mathbf{v}|_{\Omega_1} - \mathbf{v}_h$ and pressure $r_h = p|_{\Omega_2} - p_h$ in the grid analogue of the L_2-norm. The last column shows the number of iterations in the Uzawa–conjugate gradient method necessary for decreasing the residual norm up to $\varepsilon = 10^{-8}$ (the left column) and $\varepsilon = 10^{-10}$ (the right column). In the hope to obtain a more precise solution, the stop criterion of the conjugate gradient method was changed up the the value $\varepsilon = 10^{-10}$. However, this has increased the number of iterations, but has not improved the accuracy of the calculations. The data presented in the tables correspond to both cases (eight significant digits coincide). Thus, the accuracy of 10^{-10} is excessive.

6.2. The 'vortex' in the cavity (viscous fluid)

Let us consider the solution:

$$\begin{aligned} u &= \left(1-\cos\left(\frac{2\pi(\mathrm{e}^{R_1 x}-1)}{\mathrm{e}^{R_1}-1}\right)\right)\sin\left(\frac{2\pi(\mathrm{e}^{R_2 y}-1)}{\mathrm{e}^{R_2}-1}\right)\frac{R_2}{2\pi}\frac{\mathrm{e}^{R_2 y}}{(\mathrm{e}^{R_2}-1)} \\ v &= \sin\left(\frac{2\pi(\mathrm{e}^{R_1 x}-1)}{\mathrm{e}^{R_1}-1}\right)\left(1-\cos\left(\frac{2\pi(\mathrm{e}^{R_2 y}-1)}{\mathrm{e}^{R_2}-1}\right)\right)\frac{R_1}{2\pi}\frac{\mathrm{e}^{R_1 x}}{(\mathrm{e}^{R_1}-1)} \\ p &= R_1 R_2 \sin\left(\frac{2\pi(\mathrm{e}^{R_1 x}-1)}{\mathrm{e}^{R_1}-1}\right)\sin\left(\frac{2\pi(\mathrm{e}^{R_2 y}-1)}{\mathrm{e}^{R_2}-1}\right)\frac{\mathrm{e}^{R_1 x}\mathrm{e}^{R_2 y}}{(\mathrm{e}^{R_1}-1)(\mathrm{e}^{R_2}-1)}. \end{aligned} \tag{6.2}$$

Table 1.
Convergence of the difference solution and the number of iterations, example (6.1), orthogonalization.

h	$\lvert\mathbf{e}_h\rvert_{L_2}$	$\frac{\lvert\mathbf{e}_h\rvert_{L_2}}{\lvert\mathbf{e}_{2h}\rvert_{L_2}}$	$\log_2 \frac{\lvert\mathbf{e}_h\rvert_{L_2}}{\lvert\mathbf{e}_{2h}\rvert_{L_2}}$	$\lvert r_h\rvert_{L_2}$	$\frac{\lvert r_h\rvert_{L_2}}{\lvert r_{2h}\rvert_{L_2}}$	$\log_2 \frac{\lvert r_h\rvert_{L_2}}{\lvert r_{2h}\rvert_{L_2}}$	#it	#it
$1/32$	2.4860×10^{-4}	4.0116	2.0042	1.2929×10^{-3}	4.0130	2.0047	11	13
$1/64$	6.1969×10^{-5}	4.0029	2.0010	3.2218×10^{-4}	4.0033	2.0012	12	14
$1/128$	1.5481×10^{-5}	4.0007	2.0002	8.0479×10^{-5}	4.0008	2.0003	13	15
$1/256$	3.8695×10^{-6}	4.0003	2.0001	2.0115×10^{-5}	4.0000	2.0000	13	15
$1/512$	9.6730×10^{-7}			5.0288×10^{-6}			13	16

Table 2.
Convergence of the difference solution and the number of iterations, example (6.1), stabilization.

h	$\lvert\mathbf{e}_h\rvert_{L_2}$	$\frac{\lvert\mathbf{e}_h\rvert_{L_2}}{\lvert\mathbf{e}_{2h}\rvert_{L_2}}$	$\log_2 \frac{\lvert\mathbf{e}_h\rvert_{L_2}}{\lvert\mathbf{e}_{2h}\rvert_{L_2}}$	$\lvert r_h\rvert_{L_2}$	$\frac{\lvert r_h\rvert_{L_2}}{\lvert r_{2h}\rvert_{L_2}}$	$\log_2 \frac{\lvert r_h\rvert_{L_2}}{\lvert r_{2h}\rvert_{L_2}}$	#it	#it
$1/32$	2.9768×10^{-4}	3.9732	1.9903	1.9277×10^{-3}	2.9239	1.5479	13	17
$1/64$	7.4924×10^{-5}	3.9857	1.9948	6.5928×10^{-4}	2.8978	1.5350	13	17
$1/128$	1.8798×10^{-5}	3.9928	1.9974	2.2751×10^{-4}	2.8696	1.5208	13	17
$1/256$	4.7081×10^{-6}	3.9964	1.9987	7.9283×10^{-5}	2.8509	1.5114	14	17
$1/512$	1.1781×10^{-6}			2.7810×10^{-5}			14	17

The solution (6.2) imitates a 'vortex' in a cavity, the center of the vortex is at the point with the coordinates $x_0 = 1/R_1 \log(\exp(R_1) + 1)/2) \approx 0.842$, $y_0 = 1/R_2 \log(\exp(R_2) + 1)/2) \approx 0.512$. Thus, the solution has a boundary layer near the right boundary of the domain (see [2]). Figure 1 illustrates the distribution of the velocity vector (left) and the pressure field (right). The calculation results for $R_1 = 4.2985, R_2 = 0.1$ are presented in Tables 3 and 4. Table 3 contains the calculation results for the method of orthogonalization, Table 4 contains the results for the stabilized scheme. Since large gradients of velocity and pressure appear in the boundary layer, the number of iterations necessary for the convergence is greater than in the previous example. As in the first example, the solution obtained with $\varepsilon = 10^{-8}$ coincides with the solution obtained for the same approximate problem with $\varepsilon = 10^{-10}$ up to eight digits after the decimal point.

The results presented in Tables 1–4 demonstrate the second order of convergence for velocity and the same order for pressure using orthogonalization, and slightly worse using stabilization. Moreover, the number of iterations for the Uzawa–CG method with the stabilized scheme practically does not depend on the mesh size. The results of both methods are close; in the case of orthogonalization they are slightly better. Unfortunately, in the three-dimensional case the method of orthogonalization is not efficient because of the growth of the kernel dimension, but the stabilization method remains applicable.

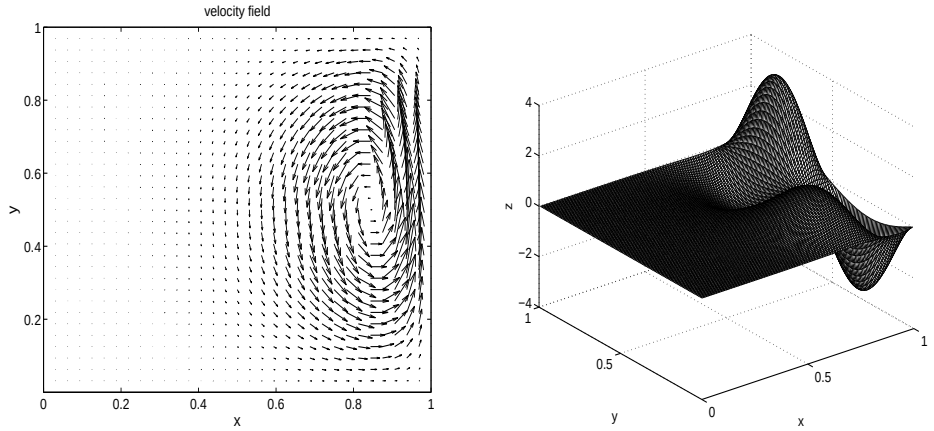

Figure 1. The velocity vector (left) and pressure (right) for example (6.2).

Table 3.
Convergence of the difference solution and the number of iterations, example (6.2), orthogonalization.

h	$\lvert\mathbf{e}_h\rvert_{L_2}$	$\frac{\lvert\mathbf{e}_h\rvert_{L_2}}{\lvert\mathbf{e}_{2h}\rvert_{L_2}}$	$\log_2 \frac{\lvert\mathbf{e}_h\rvert_{L_2}}{\lvert\mathbf{e}_{2h}\rvert_{L_2}}$	$\lvert r_h\rvert_{L_2}$	$\frac{\lvert r_h\rvert_{L_2}}{\lvert r_{2h}\rvert_{L_2}}$	$\log_2 \frac{\lvert r_h\rvert_{L_2}}{\lvert r_{2h}\rvert_{L_2}}$	#it	#it
$1/32$	7.3731×10^{-3}	4.1343	2.0476	1.3453×10^{-1}	4.3257	2.1129	14	18
$1/64$	1.7834×10^{-3}	4.0346	2.0124	3.1101×10^{-2}	4.0813	2.0290	14	19
$1/128$	4.4203×10^{-4}	4.0087	2.0031	7.6204×10^{-3}	4.0203	2.0073	14	19
$1/256$	1.1027×10^{-4}	4.0022	2.0008	1.8955×10^{-3}	4.0051	2.0018	15	19
$1/512$	2.7552×10^{-5}			4.7327×10^{-4}			15	19

Table 4.
Convergence of the difference solution and the number of iterations, example (6.2), stabilization.

h	$\lvert\mathbf{e}_h\rvert_{L_2}$	$\frac{\lvert\mathbf{e}_h\rvert_{L_2}}{\lvert\mathbf{e}_{2h}\rvert_{L_2}}$	$\log_2 \frac{\lvert\mathbf{e}_h\rvert_{L_2}}{\lvert\mathbf{e}_{2h}\rvert_{L_2}}$	$\lvert r_h\rvert_{L_2}$	$\frac{\lvert r_h\rvert_{L_2}}{\lvert r_{2h}\rvert_{L_2}}$	$\log_2 \frac{\lvert r_h\rvert_{L_2}}{\lvert r_{2h}\rvert_{L_2}}$	#it	#it
$1/32$	8.2125×10^{-3}	4.0081	2.0029	1.4631×10^{-1}	3.4115	1.7704	20	23
$1/64$	2.0490×10^{-3}	3.9559	1.9840	4.2889×10^{-2}	3.0684	1.6175	20	24
$1/128$	5.1796×10^{-4}	3.9663	1.9878	1.3977×10^{-2}	2.9778	1.5742	21	24
$1/256$	1.3059×10^{-4}	3.9808	1.9931	4.6940×10^{-3}	2.9234	1.5476	21	24
$1/512$	3.2805×10^{-5}			1.6057×10^{-3}			21	24

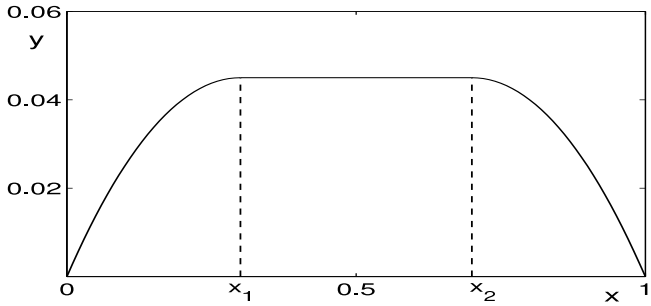

Figure 2. The velocity profile for example (6.3) with $\sigma_s = 0.2$.

6.3. Flow between plates (viscoplastic medium)

There are few analytic solutions for the models of a viscoplastic medium. Consider one of them, a flow between fixed plates (the plane Poiseuille flow):

$$v = \begin{cases} \dfrac{1}{8}[(1-2\sigma_s)^2 - (1-2\sigma_s-2x)^2], & 0 \leqslant x \leqslant x_1 \\ \dfrac{1}{8}(1-2\sigma_s)^2, & x_1 \leqslant x \leqslant x_2 \\ \dfrac{1}{8}[(1-2\sigma_s)^2 - (2x-2\sigma_s-1)^2], & \dfrac{1}{2}+\sigma_s \leqslant x \leqslant 1 \end{cases} \tag{6.3}$$

$$u = 0, \quad p = -y + \frac{1}{2}$$

where

$$x_1 = \frac{1}{2} - \sigma_s, \quad x_2 = \frac{1}{2} + \sigma_s. \tag{6.4}$$

If $\sigma_s = 0$, then we have not a viscoplastic medium, but a viscous liquid possessing a parabolic velocity profile. In the range $0 < \sigma_s < 1/2$ the velocity profile has the following form: the interval $x \in [x_1, x_2]$ corresponds to the rigid zone whose points all move at the same velocity $(1-2\sigma_s)^2/8$, in the lateral intervals $x \in [0, x_1)$ and $x \in (x_2, 1]$ a deformed medium moves. For $\sigma_s = 0.2$ the velocity profile is presented in Fig. 2. The greater σ_s, the wider is the rigid zone and the lower is the velocity. For $\sigma_s \geqslant 1/2$ we have $v = 0$, i.e., the whole domain forms a rigid fixed zone.

The dependence of the number of external iterations necessary for the convergence of Uzawa method (5.2)–(5.3) for $\mu = 1$, $\sigma_s = 0.2$, is presented in Table 5. According to estimate (4.13), the sufficient condition for the convergence of the algorithm is $0 < r < 4\mu/\sigma_s^2$. The first row presents the number of iterations in the calculation on a uniform grid with the mesh size $1/40$, the second row corresponds to the size $1/64$. For $r < 4\mu/\sigma_s^2 = 100$ the method converges, and in this case the value $r = 99.9$ requires 1024 and 1385 iterations, respectively. For $r = 100$ (and

Table 5.
The dependence of the number of iterations on the parameter r, example (6.3) with $\sigma_s = 0.2$.

h	1	10	20	30	40	50	60	70	80	90	99	99.5	99.9
$1/40$	331	164	106	80	65	55	48	43	39	36	101	204	1024
$1/64$	306	190	125	97	80	69	61	56	317	325	332	351	1385

Table 6.
The convergence of the difference solution and the number of iterations, example (6.3).

h	$\lvert\mathbf{e}_h\rvert_{L_2}$	$\frac{\lvert\mathbf{e}_h\rvert_{L_2}}{\lvert\mathbf{e}_{2h}\rvert_{L_2}}$	$\log_2 \frac{\lvert\mathbf{e}_h\rvert_{L_2}}{\lvert\mathbf{e}_{2h}\rvert_{L_2}}$	#it	$\lvert\mathbf{e}_h\rvert_{L_2}$	$\frac{\lvert\mathbf{e}_h\rvert_{L_2}}{\lvert\mathbf{e}_{2h}\rvert_{L_2}}$	$\log_2 \frac{\lvert\mathbf{e}_h\rvert_{L_2}}{\lvert\mathbf{e}_{2h}\rvert_{L_2}}$	#it
$1/20$	6.079×10^{-6}	4.2289	2.0803	28	1.668×10^{-5}	3.9311	1.9749	52
$1/40$	1.437×10^{-6}	3.4208	1.7743	48	4.244×10^{-6}	3.6274	1.8589	98
$1/80$	4.202×10^{-7}	2.7754	1.4727	88	1.170×10^{-6}	2.6495	1.4057	191
$1/160$	1.514×10^{-7}			165	4.416×10^{-7}			346

greater) we get divergence. Thus, restriction (4.13) related to the continuous problem is confirmed in numerical calculations. As can be seen, for small r the convergence is sufficiently slow, and for an r close to the right boundary of the interval it also becomes slower. The best convergence is observed for the values from the middle of the interval. Under a fixed r, the number of iterations increases for a finer grid.

Table 6 presents the values of the velocity error norm $\mathbf{e}_h = \mathbf{v}|_{\Omega_1} - \mathbf{v}_h$ in the grid analogue of the L_2-norm for example (6.3). The left half of the table corresponds to the yield stress $\sigma_s = 0.2$, $r = 60$, the right one corresponds to $\sigma_s = 0.3$, $r = 20$. The Stokes problem in internal iterations was solved by the orthogonalization method. The number of external iterations in the Uzawa method corresponds to the stopping criterion $\varepsilon = 10^{-3}$.

6.4. Driven cavity problem (viscoplastic medium)

There are two test problems for numerical algorithms solving viscoplastic problems: a flow in a pipe (the Western authors sometimes refer to it as Mosolov's problem) and a flow in a cavity. The first problem is simpler; its equivalent problem for a viscous fluid is reduced to the solution of the Poisson equation and is of great interest for mechanics. Therefore, it is solved especially often [17, 19, 21, 24]. The second problem is the best known test in computational hydrodynamics for the Stokes problem. It also becomes the test for a Bingham medium [6, 7, 10, 15, 22, 27] and consists in the following: let $\Omega = (0,1)^2$, $\mathbf{f} = 0$, the boundary conditions be given in

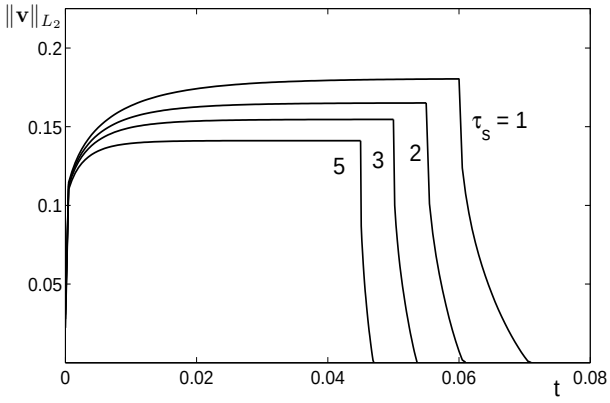

Figure 3. The velocity norm and stop time.

the following way:

$$\mathbf{v}_B(x) := \begin{cases} 0, & x \in \Gamma \setminus \Gamma_B \\ \{16(x_1^2(1-x_1)^2), 0\}, & x \in \Gamma_B. \end{cases}$$

where $\Gamma_B = \{\mathbf{x} \mid \mathbf{x} = (x_1, x_2), 0 < x_1 < 1, x_2 = 1\}$ is the moving upper boundary. This choice of the nonzero horizontal velocity component corresponds to the so-called regularized driven cavity problem.

Unsteady flows for viscoplastic media have been little studied, only one-dimensional problems were usually considered [4]. In recent papers [20, 21], numerical simulations of the unsteady flow of a Bingham medium were performed for channels of various cross-sections. An unsteady problem of the flow in a cavity was considered in [6, 7] based on the splitting method [13] with the use of FEM. In [7], rigid zones were obtained for the steady driven cavity problem, and the graph of the dependence of the velocity vector norm on time was presented for the process of the start-up of the flow (reaching the stationary state) and subsequent cessation of the flow. Let us describe these modes in more detail:

(1) Start-up of the flow: starting from the rest ($\mathbf{v}(0) = \mathbf{0}$) under the action of the instantaneously applied motion of the 'cover' of the cavity ($\mathbf{v}(t) \mid_\Gamma = \mathbf{v}_B$) the medium accelerates in the course of the time interval $(0, t_1]$, and the flow actually reaches the steady state;

(2) Cessation of the flow: from the state reached by the time moment $t = t_1$ the medium comes to a halt because the motion of the cover is 'blocked': for $t \geqslant t_1$ we have $\mathbf{v}_B(x) = 0$. The important qualitative peculiarity of the problems concerning the unsteady flows of viscoplastic media is the finiteness of the damping time of the motion in the absence of external forces [6]. This is a fundamental distinction from the corresponding flow of a viscous liquid, which damps exponentially in infinitely long time.

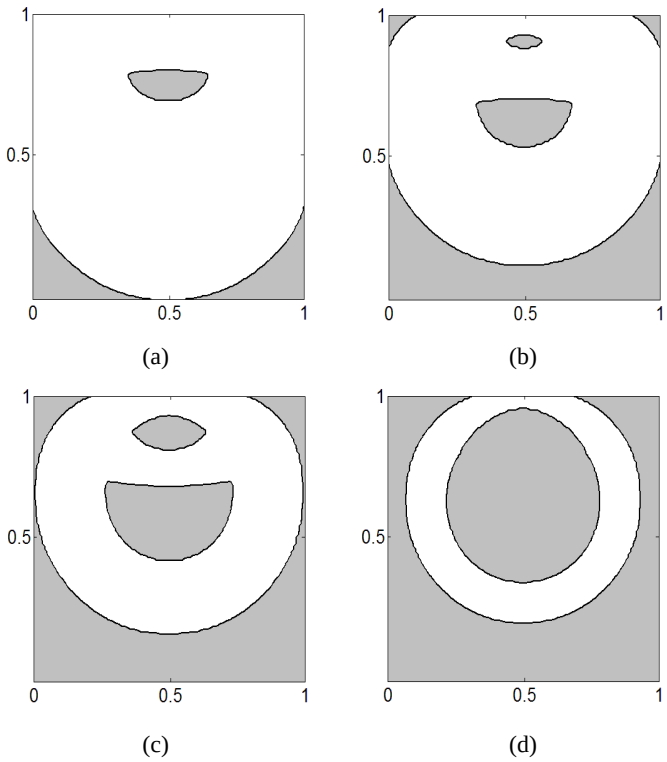

Figure 4. Development of rigid zones for $\tau_s = 1$: (a) $t = 0$, (b) $t = 0.004$, (c) $t = 0.008$, (d) $t = 0.01$.

The graphs in Fig. 3 illustrate the dependence of the velocity vector norm $\|\mathbf{v}_h\|_h$ on time. The results are presented for $\tau_s = 1\,(t_1 = 0.06)$, $\tau_s = 2\,(t_1 = 0.055)$, $\tau_s = 3\,(t_1 = 0.05)$, $\tau_s = 5\,(t_1 = 0.045)$. It is easy to see that the medium stops in a finite time interval. The curve for $\tau_s = 1$ is identical to Fig. 11 from [7].

It was noted in a classic monograph (see [10]) that 'naturally, the problem on determination of rigid zones is of most interest in numerical experiments'. Figures 4a–4d illustrate the evolution of rigid zones in time for the stopping problem. The results are presented for $\mu = 1, \rho = 1, \tau_s = 1\,(\sigma_s = \sqrt{2})$. The results were obtained on a grid with the mesh size $h = 1/128$ and the convergence criterion $\varepsilon = 10^{-4}$. Rigid zones were determined as isolines $|\boldsymbol{\tau}_h| = \sigma_s$ (the von Mises criterion is applied to the discrete field $\boldsymbol{\tau}_h$). Figure 4a corresponds to the steady flow of a viscoplastic medium in a cavity and it is in a good agreement with the previous papers [6, 7, 15, 22, 27]. Three rigid zones are present in this flow at the initial moment corresponding to the steady state. One of them is located near the center of the vortex and two others lie in the bottom part of the cavity. The bottom rigid zones gradually merge (Fig. 4b) and increase in size (Fig. 4c). The central rigid zone sinks and also increases. In the course of time (sufficiently soon) three additional rigid zone appear in the upper corners and above the central rigid zone. Some symmetry is quite natural here, because

the upper boundary of the domain becomes fixed. Further increase and merging of rigid zones progresses. Figure 4d illustrates the situation shortly before the complete stop of the flow: only a thin band of the moving medium remains between the outer (adjacent to the boundary) and the inner rigid zones. The appearance of additional rigid zones (beside those existing in the steady state) and their further merging is the typical peculiarity of unsteady flows of viscoplastic media. A similar pattern was observed when the flow in a channel was stopped [21].

7. Conclusion

In this paper we justify at the functional level the application of the Uzawa method for the solution of unsteady viscoplastic problems (without convective terms). Estimates of the convergence interval are obtained for the iterative parameter of the Uzawa method. In this case the restriction relating to the continuous problem practically coincides with the convergence interval obtained numerically in the finite-dimensional problem. The method has been implemented in a rectangular domain by a difference scheme on semi-staggered grids. Numerical experiments confirm the efficiency of the proposed approach. The evolution of rigid zones for a plane unsteady viscoplastic problem has been obtained (to best of our knowledge) for the first time and is of great interest for applied problems. In future we expect to present a more detailed justification of the application of difference approximations and the convergence of the algorithm in the finite-dimensional case, and also to extend the results to the three-dimensional unsteady case.

Acknowledgement

The authors are sincerely grateful to V. I. Agoshkov for useful comments.

References

1. M. Benzi, G. H. Golub, and J. Liesen, Numerical solution of saddle point problems. *Acta Numerica* (2005) **14**, 1–137.
2. S. Berrone, Adaptive discretization of the Navier Stokes equations by stabilized finite element methods. *Comp. Meth. Appl. Mech. Engrg.* (2001) **190**, 4435–4455.
3. P. B. Bochev, C. R. Dohrmann, and M. D. Gunzburger, Stabilization of low-order mixed finite elements for the Stokes equations. *SIAM J. Numer. Anal*. (2006) **44**, 82–101.
4. M. Chatzimina, C. Xenophontos, G. C. Georgiou, I. Argyropaidas, and E. Mitsoulis, Cessation of annular Poiseuille flows of Bingham plastics. *J. Non-Newtonian Fluid Mech.* (2007) **142**, 135–142.
5. E. V. Chizhonkov, *Relaxation Methods for Saddle Point Problems.* Moscow, INM RAS, 2002 (in Russian).
6. E. J. Dean and R. Glowinski, Operator-splitting methods for the simulation of Bingham viscoplastic flow. *Chin. Ann. Math.* (2002) **23**, 187–204.

7. E. J. Dean, R. Glowinski, and G. Guidoboni, On the numerical simulation of Bingham viscoplastic flow: Old and New results. *J. Non-Newtonian Fluid Mech.* (2007) **142**, 36–62.
8. G. Duvaut and J.-L. Lions, *Inequalities in Mechanics and Physics*. Springer, New York, 1976.
9. I. Ekeland and R. Temam, *Convex analysis and variational problems.* North-Holland, Amsterdam, 1976.
10. R. Glowinski, J.-L.Lions, and R. Tremolier'es, *Numerical Analysis of Variational Inequalities.* North Holland, Amsterdam, 1981.
11. A. A. Il'yushin, Deformation of viscoplastic body. *Uchenye Zapiski MGU. Mekhanika* (1940) **39**, 3–81 (in Russian).
12. A. V. Lapin, *Introduction into the Theory of Variational Inequalities.* KSU publishing house, Kazan, 1981 (in Russian).
13. G. I. Marchuk, *Splitting Methods*. Nauka, Moscow, 1988 (in Russian).
14. G. I. Marchuk and V. I. Agoshkov, *Introduction to Projection-grid Methods*. Nauka, Moscow, 1981 (in Russian).
15. E. Mitsoulis and Th. Zisis, Flow of Bingham plastics in a lid-driven cavity. *J. Non-Newtonian Fluid Mech.* (2001) **101**, 173–180.
16. P. P. Mosolov and V. P. Myasnikov, *Mechanics of Rigid Plastic Bodies.* Nauka, Moscow, 1981 (in Russian).
17. M. A. Moyers-Gonzalez and I. A. Frigaard, Numerical solution of duct flows of multiple viscoplastic fluids. *J. Non-Newtonian Fluid Mech.* (2004) **122**, 227–241.
18. E. A. Muravleva, On the kernel of the discrete gradient operator. *Numer. Meth. Prog.* (2008) **9**, No. 1, 97–104.
19. E. A. Muravleva, Finite-difference schemes for computation viscoplastic medium flow in channel. *Math. Model. Comp. Simulations* (2008) **20**, No. 12, 76–88.
20. E. A. Muravleva, The problem of stopping the flow of a viscoplastic medium in a channel. *Moscow Univ. Mech. Bulletin* (2009) **64**, No. 1, 25–28.
21. E. A. Muravleva and L. V. Muravleva, Unsteady flows of viscoplastic medium in channels. *Mech. Solids* (2009) **44**, No. 5, 792–812.
22. E. A. Muravleva and M. A. Olshanskii, Two finite-difference schemes for calculation of Bingham fluid flows in a cavity. *Russ. J. Numer. Anal. Math. Modelling* (2008) **23**, No. 6, 615–634.
23. E. A. Muravleva, Analysis of Scheme on Semi-staggered Grids for Stokes Problem. *Preprint of ICM*, Hong Kong (2009) (submitted).
24. N. Roquet and P. Saramito, An adaptive finite element method for viscoplastic fluid flows in pipes. *Comp. Meth. Appl. Mech. Engrg.* (2001) **190(40)**, 5391–5412.
25. A. G. Churbanov, A. N. Pavlov, and P. N. Vabishchevich, Operator-splitting method for incompressible Navier–Stokes equations on non-staggered grids. Part I: First-order schemes. *Int. J. Numer. Meth. Fluids* (1995) **21**, 617–640.
26. F. P. Vasiliev, *Optimization Methods*. Factorial Press, Moscow, 2002.
27. D. Vola, L. Boscardin, and J. C. Latche, Laminar unsteady flows of Bingham fluids: a numerical strategy and some benchmark results. *J. Comp. Phys.* (2003) **187**, 441–456.